IEEE Access
Multidisciplinary ⋮ Rapid Review ⋮ Open Access Journal

Received October 2, 2017, accepted October 29, 2017, date of publication November 14, 2017, date of current version February 14, 2018.

Digital Object Identifier 10.1109/ACCESS.2017.2773486

Robust Virtual Inertia Control of an Islanded Microgrid Considering High Penetration of Renewable Energy

THONGCHART KERDPHOL[1], (Member, IEEE), FATHIN SAIFUR RAHMAN[1], (Student Member, IEEE), YASUNORI MITANI[1], (Member, IEEE), MASAYUKI WATANABE[1], (Member, IEEE), AND SINAN KÜFEOĞLU[2]

[1]Department of Electrical and Electronic Engineering, Kyushu Institute of Technology, Kitakyushu 804-8550, Japan
[2]Institute for Sustainable Resources, University College London, London WC1E 6BT, U.K.

Corresponding author: Thongchart Kerdphol (thongchartkerd@gmail.com)

ABSTRACT This paper presents robust virtual inertia control of an islanded microgrid considering high penetration of renewable energy sources (RESs). In such microgrids, the lack of system inertia due to the replacement of traditional generating units with a large amount of RESs causes undesirable influence to microgrid frequency stability, leading to weakening of the microgrid. In order to handle this challenge, the H_∞ robust control method is implemented to the virtual inertial control loop, taking into account the high penetration of RESs, thus enhancing the robust performance and stability of the microgrid during contingencies. The controller's robustness and performance are determined along with numerous disturbances and parametric uncertainties. The comparative study between H_∞ and optimal proportional-integral (PI)-based virtual inertia controller is also presented. The results show the superior robustness and control effect of the proposed H_∞ controller in terms of precise reference frequency tracking and disturbance attenuation over the optimal PI controller. It is validated that the proposed H_∞-based virtual inertia controller successfully provides desired robust frequency support to a low-inertia islanded microgrid against high RESs penetration.

INDEX TERMS Frequency control, H_∞, islanded microgrid, renewable energy, robust control, virtual inertia control, virtual synchronous generator.

I. INTRODUCTION

Nowadays, traditional generations are being replaced by a large amount of renewable energy sources (RESs). Consequently, the inertia of islanded microgrids significantly falls and may increase variations in system frequency [1]. As RESs exchange power to microgrids via power inverters, the power electronics-based RESs will reduce the system inertia, generating high frequency and voltage fluctuation in the microgrids, compared to traditional synchronous generators. Islanded microgrids might become insecure if the RESs capacity becomes larger and larger. With the increasing RESs penetration, microgrids lack inertia, creating the difficulty in stabilizing system frequency/voltage, causing the weakening of microgrid stability and resiliency [2], [3].

Dealing with such problem, a virtual synchronous generator (VSG) concept is presented to imitate the nature of traditional generating units virtually into power systems, hence enhancing power system inertia, output impedance, microgrid stability, and resiliency [2]–[6]. Virtual inertia control is a specific part of VSG operation, where the action of a prime mover is emulated to support frequency stability [5]. The virtual inertia control employed in the energy storage systems (ESS) will enable the ESS to operate as a traditional generator, exhibiting inertia and damping properties of traditional generations to the system. The virtual inertia control can offer a basis for maintaining the share of RESs or distributed generations (DGs) in the microgrid without compromising microgrid stability and resiliency [6]. Without virtual inertia control, RESs or DGs might cause microgrid instability and cascading outages in the disturbance events.

Numerous control techniques have been implemented to virtual inertia control to solve microgrid frequency control problems, improving frequency stability [2], [7]–[12]. In [7], a classical control method employing proportional-integral (PI) control technique has been applied for virtual inertia control. The application of virtual inertia control based on

PI controller for wind power to support microgrid frequency stability is proposed in [8]. In [9] and [10], the fuzzy logic system–based virtual inertia control is applied to regulate frequency deviation in an islanded microgrid. In [11], using a virtual inertia control based on model predictive control method, the stability and robustness performance of the microgrid is investigated during high penetration of RESs. An estimation technique of frequency response based on virtual inertia control to enhance the stability of the system with high wind power integration is evaluated in [12]. Recently, a derivative control technique-based virtual inertia controller is proposed to support frequency stability in HVDC interconnected power systems [2].

Related to the former control techniques, it is not easy to obtain a proper trade-off between nominal performance and robust performance. Furthermore, the uncertainty formulation has not been considered and designed (i.e., unstructured uncertainty modeling) in the control methods [2], [7]–[12]. Therefore, it is difficult to guarantee simultaneous robust stability and performance in wide range of disturbances and uncertainties using the aforementioned control techniques. Due to the possibility of uncertainty formulation (i.e., structured uncertainty modeling) in the control synthesis procedure [13], the robust control techniques could solve this problem effectively.

The robust control approaches consider physical constraints, disturbances, and uncertainties, thus providing efficient control synthesis method for dynamic systems. However, most robust control techniques utilize complex state-feedback controllers, of which the orders are not smaller than the order of the controlled systems [14], [15]. Nevertheless, the small-scale microgrids in comparison with traditional large-scale power systems once again bring our concentration to apply these robust techniques for microgrid control issues.

Several research and studies on robust control application for microgrids have been presented in [16]–[21]. A robust frequency control method for islanded microgrids is designed in [16]. In [17], H_∞ robust controller is designed for each generation unit of a microgrid. Afterwards, the H_∞ robust controller has been designed for power-sharing in both interconnected and islanded microgrids [18]. Similar works in utilizing robust control techniques on microgrid frequency control are presented in [19] and [20]. Recently, the H_∞ robust controller is proposed to develop the secondary frequency control for microgrids [21]. To the best knowledge of the authors, there has not been any research done yet on the robust control design for virtual inertia control where uncertainties and disturbances are taken into account simultaneously. The main emphasis has been given on the development of virtual inertia control in the field of power electronics, such as equipment and control scales without concerning the effect of high penetration of RESs [2], [7]–[12]. Without considering this effect, the virtual inertia control may be insufficient and unstable for islanded microgrids, causing instability and system collapse. This is the main weakness of the previous approaches. Moreover, there is no report on the robust control strategies in the virtual inertia control for microgrids. Hence, it is expected that using the robust virtual inertia control in a new environment will be more adaptive and flexible than conventional ones in [2] and [7]–[12].

This research focuses on the new design of H_∞ robust control based on virtual inertia control loop for improving frequency stability of an islanded microgrid. The proposed robust technique is flexible enough to combine disturbances and uncertainties in the microgrid model and control process. The linear fractional transformation (LFT) method is applied in the H_∞ control design and the parametric perturbation is defined in one block as an uncertainty. Later, the robust stability and performance are investigated taking into account the high penetration of RESs. The comparative study between H_∞ and optimal PI-based virtual inertia control is also performed.

The research contribution of the robust H_∞control method in this paper over the existing the virtual inertia control loop in an islanded microgrid is that:

i. Treating the microgrid system inertia as a bounded sector of uncertainties in the H_∞ control design procedure;

ii. Treating the high penetration of RESs and loads as a bounded sector of disturbances in the H_∞ control design procedure;

iii. Designing a robust H_∞-based virtual inertia controller to minimize the frequency deviations of an islanded microgrid, enhancing microgrid stability and resiliency.

The rest of this paper is organized as follow. Section II explains the system configuration including an islanded microgrid modeling and virtual inertia control modeling. Section III describes a state-space dynamic modeling of the islanded microgrid. In section VI, the robust H_∞ control-based virtual inertia control is designed considering high penetration of RESs. The H_∞ controller order reduction is evaluated in Section V. The results of the time-domain simulations are discussed in Section VI. Finally, the conclusion is shown in Section VII.

II. SYSTEM CONFIGURATION

A. RELATION BETWEEN FREQUENCY DEVIATION AND INERTIA POWER

In this study, frequency control is divided into three main operations: the inertia control state, primary control state, and secondary control state. During the inertia control state, the controller has not initiated yet, therefore when a frequency deviation occurs, the power requirement is balanced by the kinetic energy from a generating unit. During the second state, primary control stabilizes frequency to a new steady-state condition for a time duration between 10 s to 30 s after the contingencies. Then, the secondary control, like load frequency control (LFC), recovers frequency to its nominal state of equilibrium for a time duration between 30 s and 30 minutes after the contingencies [13].

For traditional power systems, the inertia power response is represented by kinetic energy. The overall kinetic energy of the system rotational mass, including spinning loads, is calculated as [5], [13], [22]:

$$E_{kinetic} = \frac{1}{2}J\omega^2 \tag{1}$$

where J is the moment of system inertia (kgm^2) and ω is the angular frequency deviation (rad/s).

The rate of change of rotor speed depends on the torque balance of spinning mass as follows:

$$T_m - T_e = \frac{P_m}{\omega} - \frac{P_e}{\omega} = J\frac{d\omega}{dt} \tag{2}$$

where T_m and T_e are the mechanical and electrical torque, respectively. P_m and P_e are the mechanical and electrical power, respectively.

The stored kinetic energy ($E_{kinetic}$) is commonly represented proportional to its power rating and known as a system inertia constant (H) [13]:

$$H = \frac{E_{kinetic}}{S} \tag{3}$$

where S is the rated apparent power (VA).

As a common practice, the rate of change of frequency (ROCOF) of the power system is applied for modifying active power and controlling system frequency against the variation in the power demand. The ROCOF is also used to determine the inertia of power systems. Thus, the system inertia constant (H) is determined by the ROCOF as follow [13], [22]:

$$\frac{d\omega}{dt} = \frac{\omega\,(P_m - P_e)}{2HS} \tag{4}$$

B. ISLANDED MICROGRID MODELING

This research focuses on the islanded microgrid including 15 MW of domestic loads, 12 MW of a thermal power plant, 7 MW of a wind farm, 9 MW of a solar farm and 4 MW of energy storage systems (ESS) as shown in Fig. 1. The system base is 12 MW.

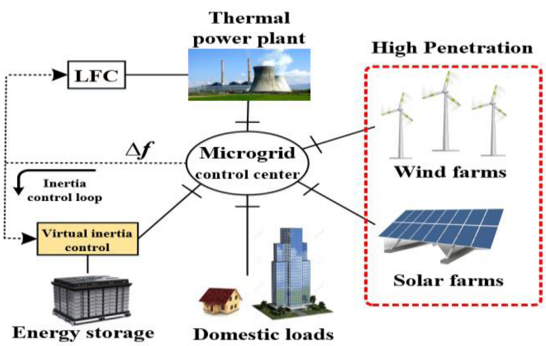

FIGURE 1. Simplified model of the islanded microgrid with high RESs penetration.

The dynamic model of the islanded microgrid is displayed in Fig 2. The microgrid parameters are presented in Table 1. To obtain the precise perception of the actual microgrid, this article also considers the significant inherent conditions and basic constraints required by the physical system dynamics of the generation and load units. The significant physical constraint of the thermal power plant is the rate of change of power generation owing to the limitation of thermal and mechanical movements. The physical system dynamics of the thermal generation is characterized by the generation rate constraint (GRC) and the maximum/minimum valve gate opening or closing for a turbine unit. The GRC of non-reheat thermal generation is set as 12% p.u. MW/minute. The V_U and V_L are the maximum and minimum limits that restrict the rate of the valve-gate closing or opening speed [13]. The significant physical constraint of the virtual inertia system is explained in the next part. The low-order dynamic models for RESs/energy storage units are explained in [13], [20], and [23]. Some type of RESs might have high-order dynamic response models, although the low-order dynamic models considered in this article are sufficient to analyze frequency control problem [13], [22], [23]. Afterwards, the wind power, solar irradiation power, and load demand are considered as the disturbance to the islanded microgrid.

TABLE 1. Dynamic parameters of islanded microgrid.

Parameters	Value
Frequency bias factor, B (p.u.MW/Hz)	1
Integral control variable gain, K_i (s)	0.05
Time constant of governor, T_g (s)	0.1
Time constant of turbine, T_t (s)	0.4
Droop constant, R (Hz/p.u.MW)	2.4
Microgrid damping coefficient, D (p.u.MW/Hz)	0.015
Microgrid system inertia, H (p.u.MW s)	0.083
Virtual inertia control gain, K_{VI} (s)	0.5
Virtual inertia time constant-based ESS, T_{VI} (s)	10
Wind turbine time constant, T_{WT} (s)	1.5
Solar system time constant, T_{PV} (s)	1.8
Maximum limit of valve gate, V_U (p.u.MW)	0.3
Minimum limit of valve gate, V_L (p.u.MW)	-0.3

C. VIRTUAL INERTIA CONTROL FOR ISLANDED MICROGRIDS

Virtual inertia control is a specific part of a virtual synchronous generator (VSG) operation, where the action of a prime mover is emulated to support frequency stability [3]–[6]. To imitate sufficient virtual inertia based on a power electronic device, the dynamic control structure is proposed in Fig. 3. The main concept of virtual inertia control is the derivative control that calculates the rate-of-change of frequency (ROCOF) to add an extra active power to the set-point of the microgrid during the contingencies. The derivative control is hypersensitive to the noise in the frequency measurement. To solve such problem, a low-pass filter is added to the control. This low-pass filter could also simulate the dynamic behavior of ESS (i.e., fast response). Consequently, the virtual inertia control system contributes to the islanded microgrid as if RESs in the islanded microgrid

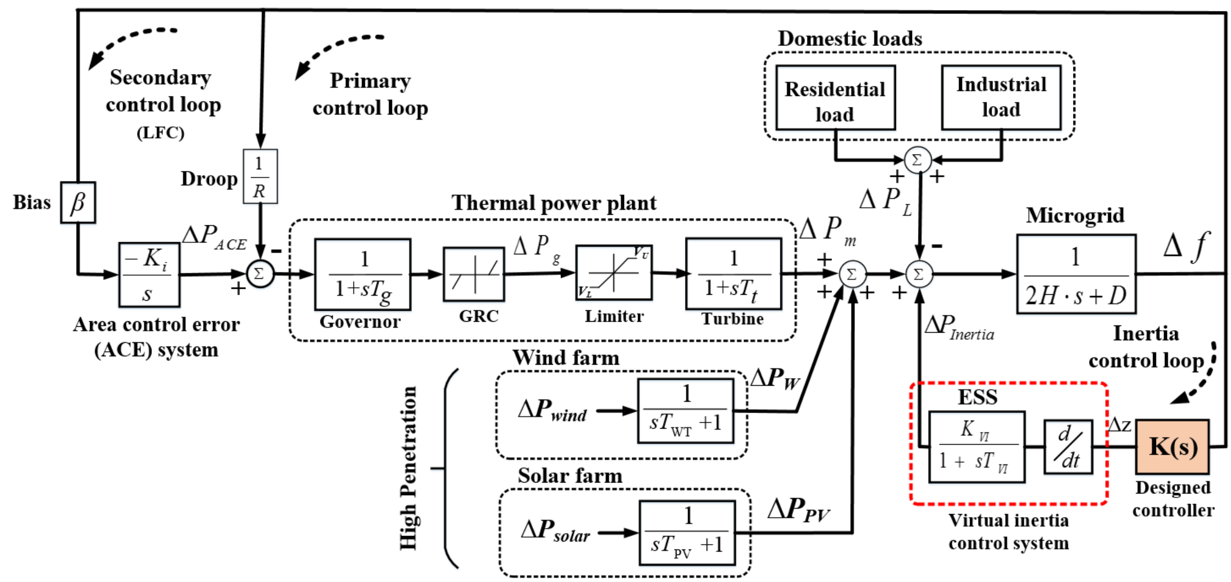

FIGURE 2. Dynamic model of the islanded microgrid considering high penetration of RESs.

would have inertia similar to the traditional generating units (i.e., synchronous generators). Thus, the virtual inertia control system imitates the inertia characteristic, contributing to the total inertia of the islanded microgrid and improving the frequency stability and resiliency. In this research, we assumed that the inertia power is emulated via the installed ESS.

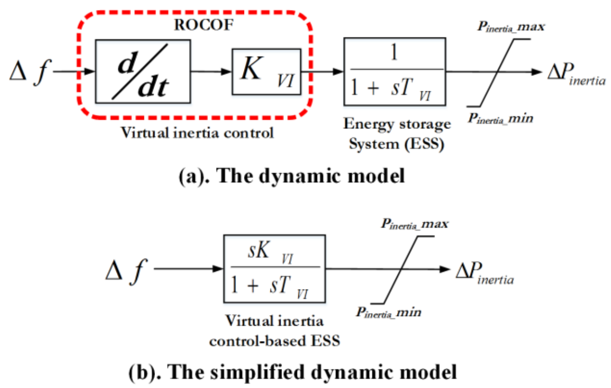

FIGURE 3. Dynamic structure of virtual inertia control.

The control law and regulation for virtual inertia power in Laplace with per-unit value is presented in Fig. 3. For any frequency deviation, the virtual inertial control system delivers the required power to the islanded microgrid as follow [2], [11], [24]:

$$\Delta P_{inertia} = \frac{K_{VI}}{1 + sT_{VI}}\left[\frac{d\,(\Delta f)}{dt}\right] \tag{5}$$

Where K_{VI} is the control gain of the virtual inertia controller and T_{VI} is the virtual inertia time constant of the added filter for emulating the dynamic control for ESS. Δf is the frequency deviation. In per unit, Δf has the same value as $\Delta\omega$.

III. STATE-SPACE DYNAMIC MODELING

The linearized state-space model is an effective model for the robust control design in microgrid control synthesis [13]. The frequency deviation of the islanded microgrid considering the effect of primary, secondary (i.e. LFC), and inertia controls can be obtained as:

$$\Delta f = \frac{1}{2Hs + D}(\Delta P_m + \Delta P_W + \Delta P_{PV} + \Delta P_{inertia} - \Delta P_L) \tag{6}$$

where,

$$\Delta P_m = \frac{1}{1 + sT_t}\left(\Delta P_g\right) \tag{7}$$

$$\Delta P_g = \frac{1}{1 + sT_g}\left(\Delta P_{ACE} - \frac{1}{R}\Delta f\right) \tag{8}$$

$$\Delta P_{ACE} = \frac{ACE}{s} = \frac{K_i}{s}\left[\beta \cdot \Delta f\right] \tag{9}$$

$$\Delta P_W = \frac{1}{1 + sT_{WT}}\left[\Delta P_{wind}\right] \tag{10}$$

$$\Delta P_{PV} = \frac{1}{1 + sT_{PV}}\left[\Delta P_{solar}\right] \tag{11}$$

$$\Delta P_{inertia} = \frac{K_{VI}}{1 + sT_{VI}}\left[\frac{d\,(\Delta f)}{dt}\right] \tag{12}$$

To perform detailed analysis, the complete state-space model representation of the islanded microgrid is important. The state-space model is given in (13) and (14) [13].

$$\dot{x} = Ax + B_1 w + B_2 u \tag{13}$$

$$y = Cx \tag{14}$$

where,

$$x^T = \begin{bmatrix} \Delta f & \Delta P_m & \Delta P_g & \Delta P_{ACE} & \Delta P_{inertia} & \Delta P_W & \Delta P_{PV} \end{bmatrix} \tag{15}$$

$$w^T = \begin{bmatrix} \Delta P_{wind} & \Delta P_{solar} & \Delta P_L \end{bmatrix} \tag{16}$$

$$y = \Delta f \tag{17}$$

In this study, wind power variation (ΔP_{wind}), solar radiation power variation (ΔP_{solar}), load power variation (ΔP_L) are considered as microgrid disturbance signals. Microgrid damping (D) and microgrid system inertia (H) are considered as the uncertain parameters. u is the signal of control input. Δf is the frequency deviation. ΔP_m is the generated power deviation of thermal power plant. ΔP_g is the governor power deviation. ΔP_{ACE} is the control signal for secondary control.

Using suitable definitions and state variables from (6)-(12), the linearized state-space model of the islanded microgrid from Fig. 2 can be simply achieved in the form of (13) and (14). Therefore, the complete state-space equations for the islanded microgrid considering high RESs penetration are obtained as in (18), as shown at the bottom of the next page.

IV. ROBUST $H\infty$ DESIGN FOR VIRTUAL INERTIA CONTROL

The main objective of this section is to describe the design of the robust controller-based virtual inertia control to imitate virtual inertia into the islanded microgrid, supporting frequency control and avoiding system collapse during contingencies. The principle of $H\infty$ control design is provided in the Appendix.

A. MODELING OF UNCERTAINTY

Microgrid behavior typically involves several uncertainties such as continuous changes in system dynamics, load and generations as well as operating microgrid condition. Hence, the uncertainty issue in microgrid operation and control has become a significant factor for microgrid control and design. In the robust control literature, various research has proposed the design of uncertainties modeling [13], [25], [30] in power systems, since the uncertainty as a dynamic perturbation can show the difference between mathematical and actual model.

For the $H\infty$ design-based virtual inertia control, dynamic perturbations considered in the studied microgrid are lumped into one perturbation block of $\Delta(s)$. Afterwards, the output multiplicative perturbation technique is applied for the uncertainty modeling. Fig. 4 displays the structure of the closed-loop microgrid system for the $H\infty$ control design process including the weighting functions and lumped uncertainty. $G(s)$ and $P(s)$ represent the nominal microgrid model without perturbation and nominal microgrid with the actual dynamics (i.e., perturbed microgrid), respectively. $K(s)$ is the $H\infty$ controller. The weighting function $W_e(s)$ has the low-pass characteristic to analyze the robust stability and the modeling error. The reason for applying a low-pass filter on the output

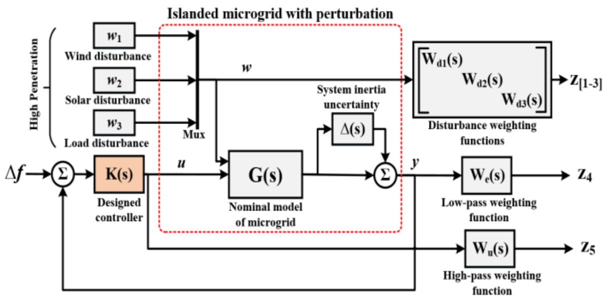

FIGURE 4. The closed-loop islanded microgrid framework including lumped multiplicative disturbance and uncertainty.

y is owing to no tracking required at very high frequencies for the microgrid frequency control system. The weighting function $W_u(s)$ has the high-pass characteristic to examine the weight on the control input u. In this study, we consider a high-integration of the wind power variation (ΔP_{wind}), the solar radiation power variation (ΔP_{solar}), and the load power variation (ΔP_L), as the disturbance. Thus, the disturbance functions $W_{d1}(s)$, $W_{d2}(s)$, and $W_{d3}(s)$ are selected to increase the robust stability and performance of the microgrid. w_1, w_2, and w_3 are the disturbance inputs from wind power, solar power, and load power variation, respectively. Z_1, Z_2, Z_3, Z_4, and Z_5 are the desired performance signals. u is the control signal from $H\infty$ controller. y is the measured output. To obtain suitable closed-loop stability margin and performance, the suitable selection of the low-pass, high-pass, and disturbance weighting functions are shown below.

$$W_e(s) = 30 \cdot \frac{s + 90}{s + 0.01} \tag{19}$$

$$W_u(s) = 0.01 \cdot \frac{0.5s + 60}{0.0001s + 20} \tag{20}$$

$$W_d(s) = \begin{bmatrix} W_{d1}(s) & 0 & 0 \\ 0 & W_{d2}(s) & 0 \\ 0 & 0 & W_{d3}(s) \end{bmatrix} = \begin{bmatrix} 0.15 & 0 & 0 \\ 0 & 0.15 & 0 \\ 0 & 0 & 0.05 \end{bmatrix} \tag{21}$$

To properly determine the weighting functions, we initially evaluate the type and objective of weighting functions (e.g., low or high pass filter). Afterwards, we begin by an initial weight and continue the tuning process concerning the closed-loop microgrid performance based on (22) in a simulation environment until reaching the desirable performance.

B. THE $H\infty$ CONTROLLER

The robust $H\infty$ controller is a remarkable control technique in dealing with non-linear tracking issues by producing a systematic method for building a robust non-linear controller. This method will evaluate a feasible robust controller by minimizing the infinite (∞)-norm of a suitable linear fractional transformation (LFT), $E(G,K)$ as follows [13]:

$$\|E(G, K)\|_\infty < 1 \tag{22}$$

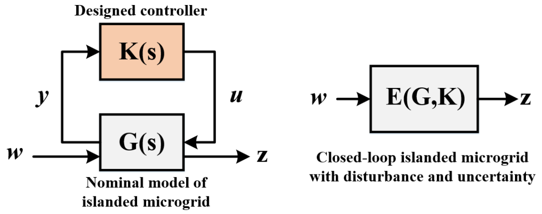

FIGURE 5. The closed-loop islanded microgrid via $H\infty$ control framework.

Fig. 5 displays the fundamental closed-loop LFT for the $H\infty$ control design. *E(G,K)* is the transfer function matrix of the nominal closed-loop microgrid system from disturbance inputs to controlled outputs, that is characterized as the transfer function T_{wz}. Based on (22), it is obvious that the optimization problem is not unique. Thus, the stabilizing $K\infty$ controller is optimally determined by the $H\infty$ norm: that is, the $H\infty$ norm of (22) must not exceed one.

C. THE CLOSED-LOOP NOMINAL STABILITY AND PERFORMANCE

The nominal stability and performance are satisfied when the closed-loop microgrid system T_{wz} is internally steady for the designed $K\infty$ controller. To evaluate the nominal stability and performance, the ∞-norm of the $K(s)$ function must be obtained less than a positive value. Using (23), the nominal stability and performance rule can be performed, where W_e W_u are the weighting functions [26], [27].

$$\left\| \begin{bmatrix} W_e\,(I+GK)^{-1} \\ W_uK\,(I+GK)^{-1} \end{bmatrix} \right\|_\infty < 1 \tag{23}$$

The specific command called *hinfsyn* in MATLAB® robust control toolbox is applied for determining the inequality from (23). From Fig. 6, it demonstrates that the ∞-norm inequality of (23) is satisfied and always not exceed one. Thus, it is confirmed that the closed-loop microgrid system effectively reduces the influence of disturbances (i.e., high penetration of wind, solar, and load power) and the desired performance is successfully achieved.

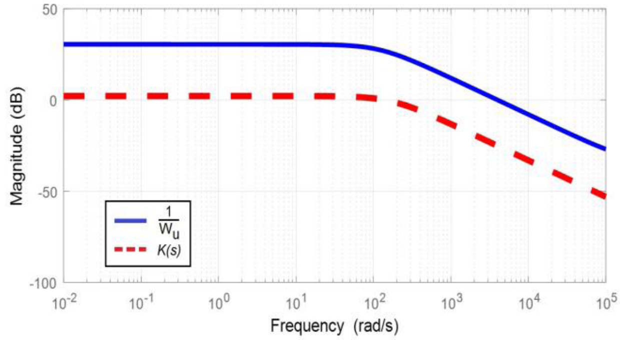

FIGURE 6. The $K(s)$ function of the nominal microgrid system.

D. THE CLOSED-LOOP ROBUST STABILITY AND PERFORMANCE

The robust stability and performance are satisfied when the closed-loop microgrid system T_{wz} is internally steady for all possible plants $P = (I + \Delta(s))G(s)$, where Δ is the uncertainty block. To evaluate the robust stability and performance, the rule of robust stability and performance must be satisfied for all possible plants P as follows [13]:

$$\left\| \begin{bmatrix} W_e\,(I+GP)^{-1} \\ W_uK\,(I+GP)^{-1} \end{bmatrix} \right\|_\infty < 1 \tag{24}$$

In this study, we consider 50% perturbations of the damping (D) and system inertia (H) values. Looking at Fig. 7, the ∞-norm inequalities calculated from (24) for all possible P are lower than one. In fact, $||[W_uK(I+GP)^{-1}]||_\infty < 1$ is also fulfilled, or $||[K(I+GP)^{-1}]||_\infty$ is less than $1/W_u$. Thus, the robust stability and performance are successfully obtained for the designed K controller through the equation of ∞-norm inequality in (24).

The design process of $K(s)$ controller is clearly explained in the following steps:

Step 1: Compute the state-space model from (18) for a given microgrid control system.

Step 2: Tune the constant weights and compute the optimum guaranteed robust performance index γ using the

$$\dot{x} = \begin{bmatrix} -\frac{D}{2H} & \frac{1}{2H} & \frac{1}{2H} & \frac{1}{2H} & \frac{1}{2H} & \frac{1}{2H} & \frac{1}{2H} \\ 0 & -\frac{1}{T_t} & \frac{1}{T_t} & 0 & 0 & 0 & 0 \\ -\frac{1}{RT_g} & 0 & -\frac{1}{T_g} & \frac{1}{T_g} & 0 & 0 & 0 \\ \beta \cdot K_i & 0 & 0 & 0 & 0 & 0 & 0 \\ 0 & 0 & 0 & 0 & -\frac{1}{T_{VI}} & 0 & 0 \\ 0 & 0 & 0 & 0 & 0 & \frac{1}{T_{WT}} & 0 \\ 0 & 0 & 0 & 0 & 0 & 0 & -\frac{1}{T_{PV}} \end{bmatrix} \begin{bmatrix} \Delta f \\ \Delta P_m \\ \Delta P_g \\ \Delta P_{ACE} \\ \Delta P_{inertia} \\ \Delta P_W \\ \Delta P_{PV} \end{bmatrix} + \begin{bmatrix} 0 & 0 & -\frac{1}{2H} \\ 0 & 0 & 0 \\ 0 & 0 & 0 \\ 0 & 0 & 0 \\ 0 & 0 & 0 \\ \frac{1}{T_{WT}} & 0 & 0 \\ 0 & \frac{1}{T_{PV}} & 0 \end{bmatrix} \begin{bmatrix} \Delta P_{wind} \\ \Delta P_{solar} \\ \Delta P_L \end{bmatrix} + \begin{bmatrix} 0 \\ 0 \\ 0 \\ 0 \\ \frac{K_{VI}}{T_{VI}} \\ 0 \\ 0 \end{bmatrix} u$$

$$y = \begin{bmatrix} 1 & 0 & 0 & 0 & 0 & 0 & 0 \end{bmatrix} x \tag{18}$$

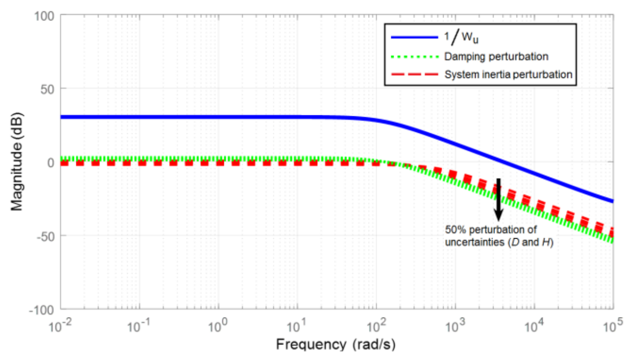

FIGURE 7. The $K(s)$ functions of the microgrid system under 50% perturbation.

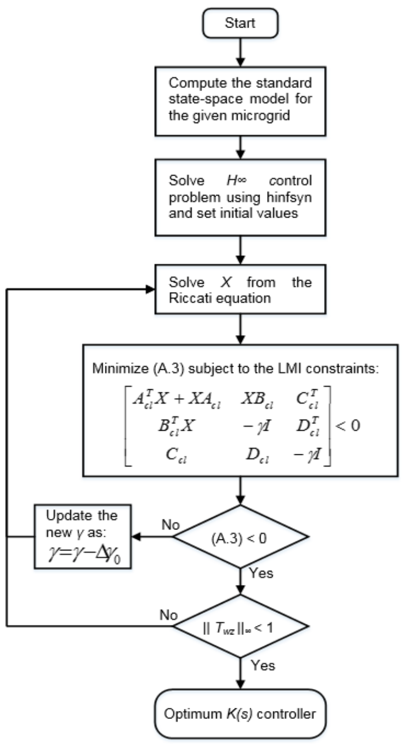

FIGURE 8. The flowchart for evaluating an optimum $K(s)$ controller.

hinfsyn command in MATLAB based on linear matrix inequality (LMI) control toolbox to design the standard robust dynamic output controller for the performed microgrid system in Step 1. Then, set $\Delta\gamma = \Delta\gamma_0$ and let $\gamma = \gamma_0$ for an initial iteration. In addition, γ_0 and $\Delta\gamma_0$ are the positive real number.

Step 3: Solve a system matrix X from the Riccati equation.

Step 4: Minimize (A.3) subject to the LMI constraints.

Step 5: If (A.3) < 0, go to Step 6. Otherwise, calculate a new γ for a next iteration and go to Step 3.

Step 6: If $||T_{wz}||_\infty < 1$, $K(s)$ is an optimum $H\infty$ controller such that the obtained controller satisfies (22). Else, go to Step 3.

The design process of $K(s)$ controller is schematically described in Fig. 8.

TABLE 2. The coefficients of $H\infty$-based virtual inertia controller.

a_6	274.3	b_6	2.188×10^4
a_5	1.856×10^4	b_5	2.783×10^6
a_4	1.975×10^5	b_4	8.049×10^7
a_3	3.837×10^5	b_3	6.682×10^8
a_2	3979	b_2	1.215×10^9
a_1	1.635	b_1	1.148×10^6
a_0	0.0001473	b_0	240.2

V. $H\infty$ CONTROLLER ORDER REDUCTION

Heretofore, a high-order of the designed $H\infty$ controller has been one of the major problems of robust control techniques, particularly for the high-order plants. Using these robust control methods, the designed controller is larger than or at least equal to the order of the given plants. This problem results in difficulties for practical controller implementation. To avoid this difficulty, several techniques are proposed for order reduction [14], [28]–[30]. In this study, the Hankel optimal model order reduction [14] is implemented to reduce a high order of the $H\infty$ controller, evaluating reasonable performance and stability.

The designed controller order using the $H\infty$ control technique was originally 7th order. The designed $H\infty$ controller with the full-order is derived in the following form:

$$K(s) = \frac{b_6 s^6 + b_5 s^5 + \ldots + b_1 s + b_0}{s^7 + a_6 s^6 + a_5 s^5 + \ldots + a_1 s + a_0} \tag{25}$$

The coefficients of the designed $H\infty$ controller in the form of (25) are shown in Table. 2.

Applying the Hankel optimal model order reduction, the $H\infty$ controller order is properly reduced to 4th order. Fig. 9 displays the bode plot of the full-order (original) and reduced-order for the designed $H\infty$ controller. It is obvious that the high-order controller is reduced to the low order controller without performance deterioration. The transfer function of the reduced-order $H\infty$ controller in the form of (25) is obtained as follow:

$$K(s) = \frac{2.189\times10^4 s^3 + 2.508\times10^6 s^2 + 4.846\times10^7 s + 3.177\times10^4}{s^4 + 261.8 s^3 + 1.525\times10^4 s^2 + 154.4 s + 0.01941} \tag{26}$$

VI. RESULTS OF TIME-DOMAIN SIMULATION

The time-domain simulation during the high penetration of RESs and loads (i.e., disturbances) and parameter perturbation are performed using MATLAB/Simulink. To evaluate the efficiency of the proposed robust $H\infty$ method (reduced-order), it is compared with the optimum PI controller. The optimum PI parameters are calculated by the internal model control (IMC) method for tuning PI/PID controller [15]. The IMC technique provides the designer the flexibility in considering the modeling errors and desirable performance, disturbance rejection, and reference tracking against system

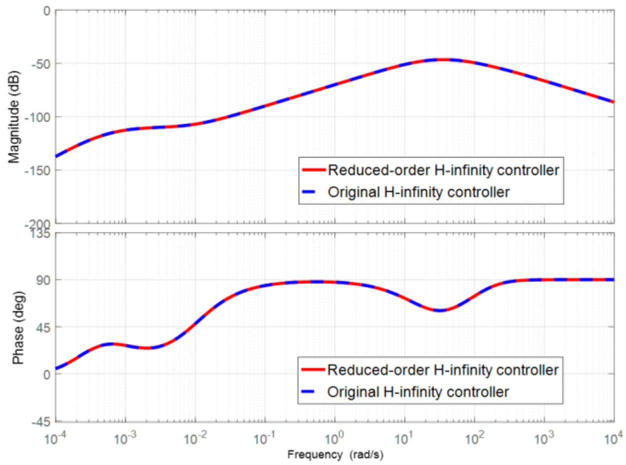

FIGURE 9. **The comparison between original (dashed) and reduced-order (solid) $H\infty$ controller.**

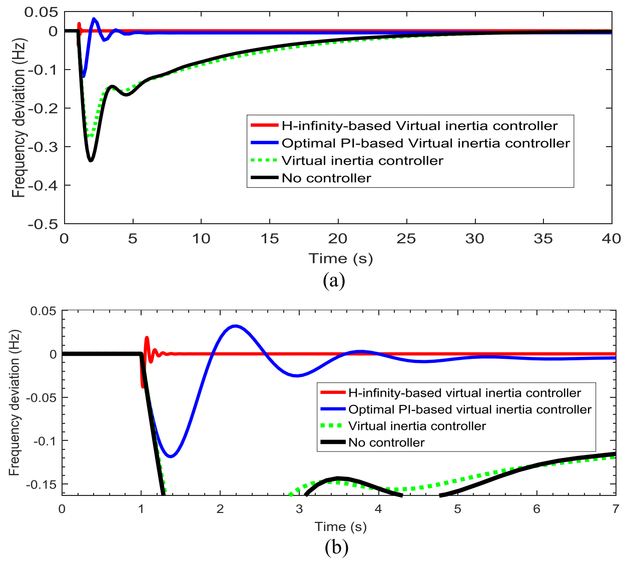

FIGURE 10. **Microgrid frequency deviation: (a) Under normal system inertia, (b) Comparison between $H\infty$ and optimal PI controllers under the normal situation of system inertia.**

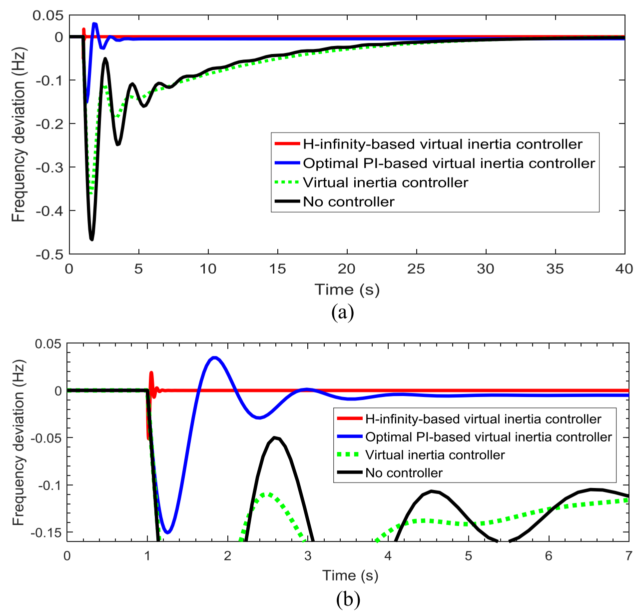

FIGURE 11. **Microgrid frequency deviation: (a) Under 50% reduction of system inertia, (b) Comparison between $H\infty$ and optimal PI controllers in the presence of 50% reduction in system inertia.**

variation and modeling error. Afterwards, the optimal parameters of K_P and K_I are obtained as 3.581 and 22.114, respectively using the MATLAB-based IMC tuning toolbox. For examining the microgrid frequency response, five severe test scenarios are conducted.

A. ABRUPT LOAD CHANGE

Scenario 1: A 10% step change of load power demand is applied under normal microgrid system inertia condition (i.e., 100% of its nominal value). Fig. 10(a) shows that the virtual inertia controller can improve the frequency performance and reduces transient excursion compared with the islanded microgrid without the virtual inertia controller. It is obvious that frequency performance is significantly enhanced by the $H\infty$-based virtual inertia controller.

For a clear comparison, a zoom view of frequency response for $H\infty$ and optimal PI-based controllers is shown in Fig. 10(b). It can be seen that $H\infty$-based virtual inertia controller performs remarkable performance in the aspect of disturbance rejection, tracking property, and zero steady-state error compared with the optimal PI-based virtual inertia controller. Thus, microgrid frequency performance is greatly enhanced by the $H\infty$–based virtual inertia controller compared to the optimal PI controller. The optimal PI controller results in considerably larger oscillating overshoot and larger transient frequency deviation.

Scenario 2: A 10% step change of load power demand is applied to the situation of 50% decrease in microgrid system inertia (as uncertainties). The effect of the microgrid frequency performance against system inertia reduction is investigated. Fig. 11(a) shows that the microgrid frequency performance is more fluctuating and larger transient deviation is observed during low system inertia condition.

Focusing on the disturbance rejection, tracking property, and error minimization during low system inertia condition in Fig. 11(b), it can be seen that more favorable result can be achieved by the $H\infty$–based virtual inertia controller. During low system inertia condition, the result indicates that the designed $H\infty$ controller is more efficient in handling the sudden load change and tracks the operating point of the islanded microgrid better compared to the optimal PI-based virtual inertia controller.

B. HIGH PENETRATION OF RESS AND LOADS

Variety in nature of RESs, generation/load, and continuous changes of system operation are known as the important characteristics of the actual microgrids. Based on

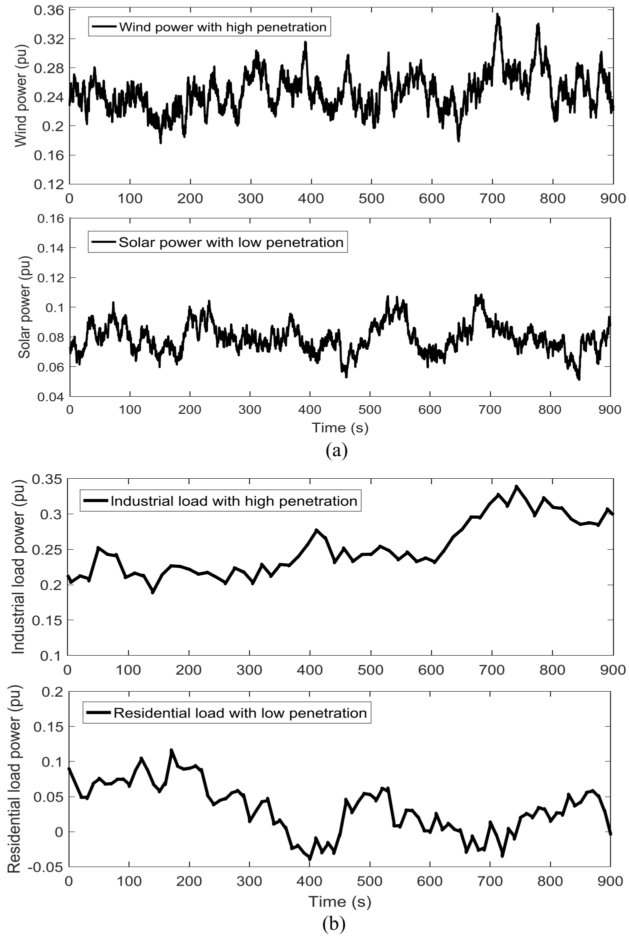

FIGURE 12. **Power variation pattern: (a) Wind and solar generations, (b) Industrial and residential load demands.**

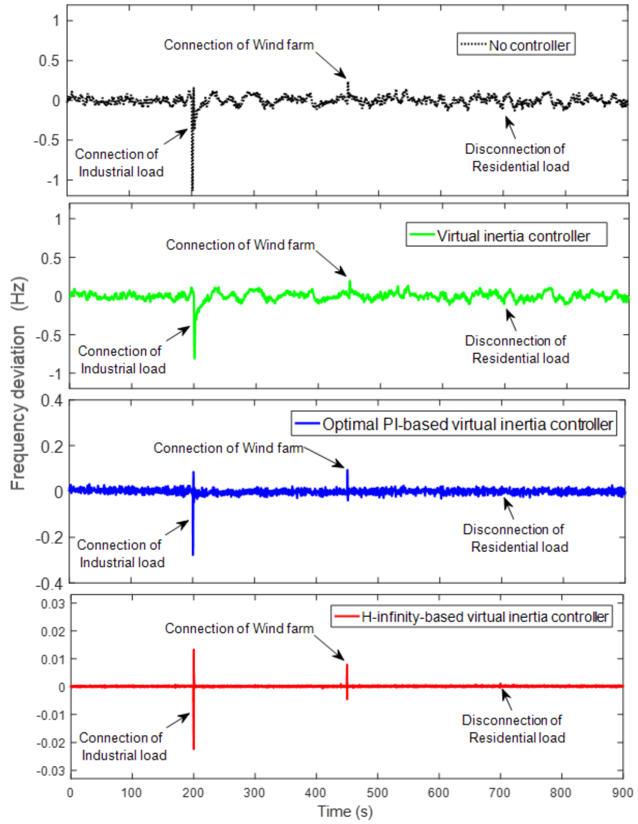

FIGURE 13. **Microgrid frequency deviation during high system inertia (i.e., reduced to 95% of its nominal value).**

TABLE 3. **Multiple Operating conditions of islanded microgrid.**

Disturbance source	Starting time (s)	Stopping time (s)	Size (MW)
Wind farm	450	-	5
Solar farm	initial	-	1.65
Residential load	initial	700	5.3
Industrial load	200	-	1.5

Scenarios 3, 4, and 5, the islanded microgrid is tested under a condition of low penetration of solar farm, high penetration of wind farm, low fluctuated load demand (i.e., residential load), and high fluctuated load demand (i.e., industrial load) as shown in Fig. 12. These severe operating conditions (See Table. 3) can represent the significant effect of actual islanded microgrid operations and test the robustness of the proposed controller against the high penetration of RESs and load, as well as system inertia variation. Thus, the impact of high RESs integration on the overall microgrid frequency behavior can be clearly seen from such test scenarios.

Scenario 3: The microgrid frequency response under the normal system inertia (i.e., 95% of its nominal value) is examined. Fig. 13 shows that the frequency response is affected by the RESs and load power fluctuations. Without the controller, the microgrid frequency has driven to a large frequency fluctuation of about ±1.1 Hz. The conventional virtual inertia controller could regulate the frequency deviation within ±0.7 Hz. The $H\infty$-based virtual inertia controller could properly maintain the frequency deviation within ±0.05 Hz while the optimal PI-based virtual inertia controller gives the frequency deviation of about ±0.25 Hz. It is obvious that the best result is obtained from the $H\infty$-based virtual inertia controller.

Scenario 4: To make the scenario more drastic, the islanded microgrid is operated under the condition of 55% reduction in system inertia. During the high penetration of RESs and loads, it is shown that the microgrid frequency response is more fluctuating with higher deviation following the system inertia reduction (See Fig. 14). It is obvious that the lack of system inertia due to high RESs penetration is particularly affecting the stability of islanded microgrids. During the connection of industrial load at 200 s, it causes a large frequency transient about −1.2 Hz in the case of the conventional virtual inertia controller (it might cause under-frequency load shedding), and about −0.4 Hz in the case of the optimal PI-based virtual inertia controller. The proposed $H\infty$ controller can properly maintain the deviation within the acceptable range of ±0.05 Hz. Without the virtual inertia controller, microgrid

TABLE 4. Evaluation indices of islanded microgrid frequency deviation.

Scenario	Microgrid system inertia	Mean absolute frequency deviation (Hz)			
		No controller	Virtual inertia controller	Optimal PI-based virtual inertia controller	$H\infty$-based virtual inertia controller
3	High (95%)	0.04878	0.04481	0.00867	0.000175
4	Medium (45%)	4.02134	0.04713	0.00905	0.000176
5	Low (15%)	13.8414	0.06467	0.00953	0.000192

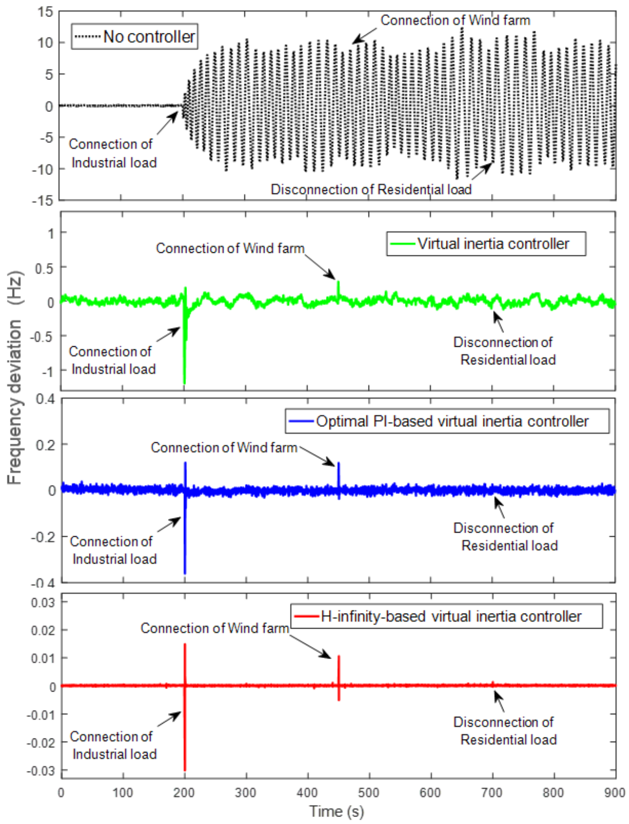

FIGURE 14. Microgrid frequency deviation during medium system inertia (i.e., reduced to 45% of its nominal value).

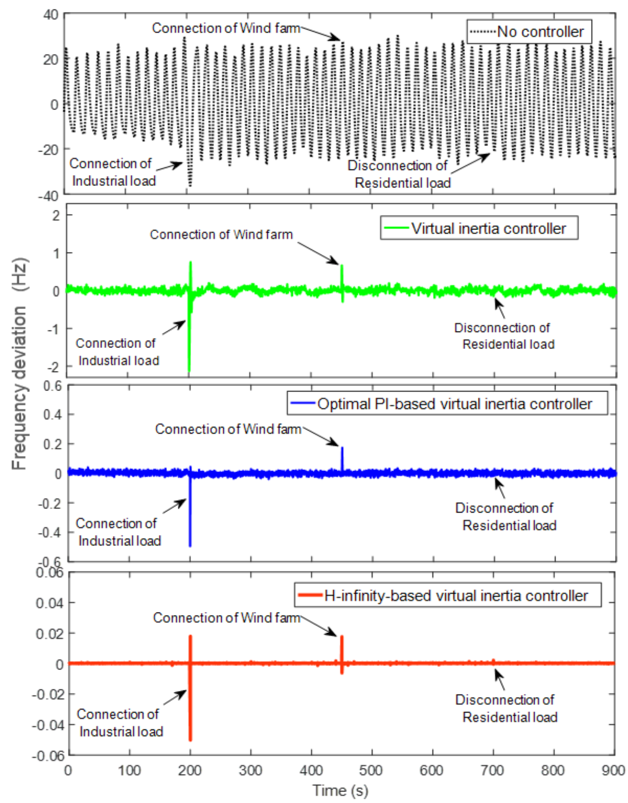

FIGURE 15. Microgrid frequency deviation during low system inertia (i.e., reduced to 15% of its nominal value) and mismatch parameters of microgrid generation.

frequency response turns into instability and, in the worst case, may lead to the cascading outages after the connection of industrial load.

Scenario 5: To perform a severe test scenario, both the thermal generation governor and turbine time constants are increased to $T_g = 0.15$ s (i.e., increased by 50% of its nominal value) and $T_t = 1.1$ s (i.e., increased by 90% of its nominal value). This phenomenon could happen in the case of off-line change of the practical turbine and governor, while the controller keeps the nominal values of these parts. It means that the thermal power plant is changed to unstable mode. Moreover, the islanded microgrid is operated under the critical condition of low system inertia (i.e., reduced to 15% of its nominal value). Fig. 15 demonstrates the microgrid frequency response under the severe condition of uncertainties. It can be seen that the frequency drop has significantly increased due to low system inertia. The lower inertia value causes a larger frequency drop. Without the virtual inertia controller, microgrid frequency cannot maintain the stability against the high integration of RESs and loads, leading to instability and system collapse. For conventional virtual inertia and optimal PI controllers, both controllers give larger oscillating overshoot and larger transient frequency deviation, resulting in a higher range of frequency fluctuation (it could cause the tripping of frequency relays and under-frequency load shedding). At this severe operating condition, the $H\infty$-based virtual inertia controller can handle the applied uncertainties and frequency deviation is abruptly driven to zero, resulting in a smaller transient of about ± 0.05 Hz (within the acceptable range) compared with the other controllers. These results suggest that the proposed robust $H\infty$ control technique may have a large potential in the control of the virtual inertia controller for microgrids.

Table. 4 shows absolute maximum frequency deviation of Scenarios 3, 4 and 5, when the microgrid system inertia is set as high, medium, and low, respectively. It can be seen that when the microgrid system inertia decreases, the maximum frequency deviation of the islanded microgrid increases. Clearly, the absolute maximum frequency deviation of the proposed $H\infty$–based virtual inertia controller is lower than those of optimal PI and conventional virtual inertia controllers for all test scenarios. These results imply that the proposed $H\infty$–based virtual inertia controller is robust to system inertia variation, high penetration of RESs power, and severe load changes.

VII. CONCLUSION

With an increasing level of RESs penetration, the lack of system inertia is particularly affecting the stability of isolated microgrids, resulting in instability, and in the worst case, it can lead to cascading outages. This issue is significant concerning the increase of the amount of installed RESs in today and future power systems/microgrids worldwide. In this research, the robust $H\infty$ technique is implemented to virtual inertia control problem concerning the high penetration of RESs for supporting frequency stability in an islanded microgrid. The $H\infty$-based virtual inertia controller is designed to reduce the influence of the wind and solar power fluctuation, load disturbances, as well as dynamic perturbation (i.e., microgrid system inertia and damping). The time-domain simulation results reveal that the proposed $H\infty$-based virtual inertia controller can effectively regulate the microgrid frequency and guarantee robust performance, such as precise reference frequency tracking and disturbance attenuation under a wide range of high RESs fluctuation, severe load disturbances, and system inertia variation. In comparison with the optimal PI-based virtual inertia controller, the reduced-order $H\infty$ controller dramatically improves the microgrid frequency control performance, enhancing microgrid stability and resiliency.

APPENDIX

This section describes a brief overview of robust $H\infty$ control theorem. The overall details and proofs can be found in [13]. Considering a linear time-invariant system $G(s)$, the following state-space realization is expressed as:

$$\begin{aligned} \dot{x} &= Ax + B_1 w + B_2 u \\ z &= C_1 x + D_{12} u \\ y &= C_2 x \end{aligned} \tag{A.1}$$

where x is the state variable vector, z is the controlled output vector, w is the disturbance and other external input vectors, and y is the measured output vector.

Using the theorem in (A.1), it is supposed that (A, B_2, C_2) is stabilizable and measurable. The $H\infty$ control problem for the linear time-invariant system $G(s)$ with the state-space realization of (A.1) is to determine a controller $K(s)$ such that the resulted closed-loop system is internally stable, and the ∞-norm of the transfer function from w to z does not exceed γ, a specified positive number as shown in [13]:

$$\|T_{wz}(s)\|_\infty < \gamma \tag{A.2}$$

Implementing matrix representation, the matrix K is the dynamic $H\infty$ controller, if and only if there is a symmetric matrix $X > 0$ such that [10]:

$$\begin{bmatrix} A_{cl}^T X + X A_{cl} & X B_{cl} & C_{cl}^T \\ B_{cl}^T X & -\gamma I & D_{cl}^T \\ C_{cl} & D_{cl} & -\gamma I \end{bmatrix} < 0 \tag{A.3}$$

where

$$\begin{aligned} A_{cl} &= A + B_2 K C_2, \quad B_{cl} = B_1 \\ C_{cl} &= C_1 + D_{12} K C_2, \quad D_{cl} = [0]. \end{aligned}$$

The proof of (A.3) is given in [13].

ACKNOWLEDGMENT

The authors are thankful for the feedbacks of anonymous reviewers, Prof. Michael Pecht, Editor-in-Chief of this journal, Dr. Flavia Grassi, Associate Editor, and Margery Meyer; their comments helped us a lot in improving the quality of this paper.

REFERENCES

[1] H. Bevrani, M. Watanabe, and Y. Mitani, *Power System Monitoring and Control*. Hoboken, NJ, USA: Wiley, Jun. 2014.

[2] E. Rakhshani, D. Remon, A. Cantarellas, and P. Rodriguez, "Analysis of derivative control based virtual inertia in multi-area high-voltage direct current interconnected power systems," *IET Generat., Trans. Distrib.*, vol. 10, no. 6, pp. 1458–1469, May 2016.

[3] H. Bevrani, T. Ise, and Y. Miura, "Virtual synchronous generators: A survey and new perspectives," *Int. J. Elect. Power Energy Syst.*, vol. 54, pp. 244–254, Jan. 2014.

[4] M. A. Torres L, L. A. C. Lopes, L. A. Morán T, and J. R. Espinoza C, "Self-tuning virtual synchronous machine: A control strategy for energy storage systems to support dynamic frequency control," *IEEE Trans. Energy Convers.*, vol. 29, no. 4, pp. 833–840, Dec. 2014.

[5] D. Li, Q. Zhu, S. Lin, and X. Y. Bian, "A self-adaptive inertia and damping combination control of VSG to support frequency stability," *IEEE Trans. Energy Convers.*, vol. 32, no. 1, pp. 397–398, Mar. 2016.

[6] H. Zhao, Q. Yang, and H. Zeng, "Multi-loop virtual synchronous generator control of inverter-based DGs under microgrid dynamics," *IET Generat., Trans. Distrib.*, vol. 11, no. 3, pp. 795–803, Feb. 2017.

[7] P. F. Frack, P. E. Mercado, and M. G. Molina, "Extending the VISMA concept to improve the frequency stability in microgrids," in *Proc. IEEE Intell. Syst. Appl. Power Syst. Conf.*, Sep. 2015, pp. 1–6.

[8] E. Chikuni, F. F. Gonzalez-Longatt, and E. Rashayi, "Effects of the synthesis inertia from wind power on the total system inertia after a frequency disturbance," in *Proc. IEEE Ind. Technol. Conf.*, Feb. 2013, pp. 826–832.

[9] K. Mentesidi, R. Garde, M. Aguado, and E. Rikos, "Implementation of a fuzzy logic controller for virtual inertia emulation," in *Proc. IEEE Smart Electr. Distrib. Syst. Technol. Conf.*, Sep. 2015, pp. 606–611.

[10] Y. Hu, W. Wei, Y. Peng, and J. Lei, "Fuzzy virtual inertia control for virtual synchronous generator," in *Proc. Chin. Control Conf.*, Jul. 2016, pp. 8523–8527.

[11] T. Kerdphol, F. S. Rahman, Y. Mitani, K. Hongesombut, and K. Küfeoğlu, "Virtual inertia control-based model predictive control for microgrid frequency stabilization considering high renewable energy integration," *Sustainability*, vol. 9, no. 5, p. 773, May 2017.

[12] R. Yan and T. K. Saha, "Frequency response estimation method for high wind penetration considering wind turbine frequency support functions," *IET Renew. Power Generat.*, vol. 9, no. 7, pp. 775–782, Aug. 2015.

[13] H. Bevrani, *Robust Power System Frequency Control*. 2nd ed. Gewerbestrasse, Switzerland: Springer, 2014.

[14] D. W. Gu, P. H. Petkov, and M. M. Konstantinov, *Robust Control Design With MATLAB*. New York, NY, USA: Springer, 2005.

[15] M. Morari and E. Zafirion, *Robust Process Control*. Englewood Cliffs, NJ, USA: Prentice-Hall, 1989.

[16] A. H. Etemadi, E. J. Davison, and R. Iravani, "A decentralized robust control strategy for multi-DER microgrids—Part I: Fundamental concepts," *IEEE Trans. Power Del.*, vol. 27, no. 4, pp. 1843–1853, Oct. 2012.
[17] Y. Han, P. M. Young, A. Jain, and D. Zimmerle, "Robust control for microgrid frequency deviation reduction with attached storage system," *IEEE Trans. Smart Grid*, vol. 6, no. 2, pp. 557–565, Mar. 2015.
[18] M. J. Hossain, H. R. Pota, M. A. Mahmud, and M. Aldeen, "Robust control for power sharing in microgrids with low-inertia wind and PV generators," *IEEE Trans. Sustain. Energy*, vol. 6, no. 3, pp. 1067–1077, Jul. 2014.
[19] M. Babazadeh and H. Karimi, "A robust two-degree-of-freedom control strategy for an islanded microgrid," *IEEE Trans. Power Del.*, vol. 28, no. 3, pp. 1339–1347, Jul. 2013.
[20] D.-J. Lee and L. Wang, "Small-signal stability analysis of an autonomous hybrid renewable energy power generation/energy storage system part I: Time-domain simulations," *IEEE Trans. Energy Convers.*, vol. 23, no. 1, pp. 311–320, Mar. 2008.
[21] H. Bevrani, M. R. Feizi, and S. Ataee, "Robust frequency control in an islanded microgrid: H_∞ and μ-synthesis approaches," *IEEE Trans. Smart Grid*, vol. 7, no. 2, pp. 706–717, Mar. 2016.
[22] P. Kunder, *Power System Stability and Control*. New York, NY, USA: McGraw-Hill, 1994.
[23] H. Bevrani, F. Habibi, P. Babahajyani, M. Watanabe, and Y. Mitani, "Intelligent frequency control in an AC microgrid: Online PSO-based fuzzy tuning approach," *IEEE Trans. Smart Grid*, vol. 3, no. 4, pp. 1935–1944, Dec. 2012.
[24] M. Datta, H. Ishikawa, H. Naitoh, and T. Senjyu, "Frequency control improvement in a PV-diesel hybrid power system with a virtual inertia controller," in *Proc. IEEE Ind. Electron. Appl. Conf.*, Jul. 2012, pp. 1167–1172.
[25] A. Packard and J. Doyle, "The complex structured singular value," *Automatica*, vol. 29, no. 1, pp. 71–109, 1993.
[26] S. Vachirasricirikul and I. Ngamroo, "Robust controller design of heat pump and plug-in hybrid electric vehicle for frequency control in a smart microgrid based on specified-structure mixed H_2/H_∞ control technique," *Appl. Energy*, vol. 88, no. 11, pp. 3860–3868, Nov. 2011.
[27] X. Li, Y.-J. Song, and S.-B. Han, "Frequency control in micro-grid power system combined with electrolyzer system and fuzzy PI controller," *J. Power Sources*, vol. 18, no. 1, pp. 468–475, May 2008.
[28] P. Apkarian, H. D. Tuan, and D. Noll, "Fixed-order H_∞ control design via a partially augmented Lagrangian method," *Int. J. Robust Nonlinear Control*, vol. 13, no. 12, pp. 1137–1148, Jun. 2003.
[29] M. P. S. Gryning, Q. Wu, M. Blanke, H. H. Niemann, and K. P. H. Andersen, "Wind turbine inverter robust loop-shaping control subject to grid interaction effects," *IEEE Trans. Sustain. Energy*, vol. 7, no. 1, pp. 41–50, Jan. 2016.
[30] H. Bevrani, Y. Mitani, and K. Tsuji, "Robust decentralized AGC in a restructured power system," *Energy Convers. Manage.*, vol. 45, nos. 15–16, pp. 2297–2312, Sep. 2004.

THONGCHART KERDPHOL (S'14–M'16) received the B.Eng. and M.Eng. degrees in electrical engineering from Kasetsart University, Bangkok, Thailand, in 2010 and 2012, respectively, and the Ph.D. degree in electrical and electronic engineering from the Kyushu Institute of Technology, Kitakyushu, Japan, in 2016.

He is currently the Post-Doctoral Fellow with the Power System and Renewable Energy Laboratory (MITANI Lab), Kyushu Institute of Technology. His research interests include power system stability, robust power system control, intelligent optimization, and smart/micro-grid control.

FATHIN SAIFUR RAHMAN (S'15) received the B.Sc. degree in electrical power engineering and the M.Sc. degree in electrical engineering from the Institut Teknologi Bandung, Indonesia, in 2012 and 2013, respectively.

He is currently pursuing the Ph.D. degree with the MITANI Laboratory, Kyushu Institute of Technology. His research interest includes power system stability, smart grid and clean energy, optimization in power system, and the application of synchrophasor in power system.

YASUNORI MITANI (M'87) received the B.Sc., M.Sc., and D.Eng. degrees in electrical engineering from Osaka University, Japan, in 1981, 1983, and 1986, respectively. From 1994 to 1995, he was a Visiting Research Associate with the University of California at Berkeley, Berkeley, CA, USA.

He is currently a Professor with the Department of Electrical and Electronic Engineering, and the Director of the Industry-Academic Collaboration Division, Kyushu Institute of Technology, Japan. He is also the President of the Institute of Electrical Engineers of Japan, Power and Energy Society. He has authored several books/book chapters, and over 200 journal/conference papers. His research interests are in the areas of power system stability, dynamics, and control.

MASAYUKI WATANABE (S'03–M'05) received the B.Sc., M.Sc., and Dr. Eng. degrees in electrical engineering from Osaka University, Japan, in 2001, 2002, and 2004, respectively.

He is currently an Associate Professor with the Department of Electrical and Electronic Engineering, Kyushu Institute of Technology, Japan. He has authored books/book chapters, and over 70 journal/conference papers. His research interest is in the area of the analysis of power systems.

SINAN KÜFEOĞLU received the B.Sc. degree in electrical and electronics engineering from Middle East Technical University, Ankara, Turkey, in 2009, and the M.Sc. and D.Sc. degrees from the School of Electrical Engineering, Aalto University, Espoo, Finland, in 2011 and 2015, respectively.

Since 2017, he has been with the Institute for Sustainable Resources, University College London, U.K., as an Honorary Research Associate. His research interests include electric power reliability and customer interruption costs.